JOURNAL OF COMPUTATIONAL PHYSICS **126,** 356–372 (1996)
ARTICLE NO. 0143

Elimination of Adaptive Grid Interface Errors in the Discrete Cell Centered Pressure Equation

MICHAEL G. EDWARDS

Center for Petroleum and Geosystems Engineering, The University of Texas at Austin, Austin, Texas 78712

Received December 23, 1993; revised January 26, 1996

Classical cell centered discretization of the reservoir simulation pressure equation on an h-adaptive grid results in an $O(1/h)$ leading truncation error at the grid interface. A new flux continuous finite volume correction is presented together with an improved version of a previously proposed correction. While both corrections eliminate the leading error, the new correction exhibits the best convergence rates and has the following properties: the resulting matrix is in general symmetric positive definite, diagonally dominant for locally isotropic spatially varying coefficients, convergence to $O(h)$ is demonstrated, and support of the standard approximation is retained, ensuring a fully implicit implementation. Results computed by the uncorrected classical scheme and both correction schemes are compared for two phase flow simulations with multilevel dynamic local grid refinement.

1. INTRODUCTION

Reservoir simulation involves solving a coupled system of hyperbolic or parabolic conservation laws for component densities and an elliptic or parabolic equation for the pressure. The coupling between the equations is via the fluid velocity, defined by Darcys law to be proportional to the pressure gradient. Analogous mixed systems of partial differential equations occur in other areas of fluid dynamics such as the incompressible Euler and Navier–Stokes equations, and the techniques discussed here are applicable in those areas. The particular equation set solved here is described in the results section.

The desire to perform increasingly finer scale simulations is growing with developments in computer hardware and reservoir description techniques. The general spatial distribution of reservoir rock properties such as permeability and porosity are provided by reservoir description techniques, which generate fine scale permeability maps (or realizations) by statistical techniques according to known geological data, seismic, and well measurements. The multitude of fine scale realizations increases both the number of simulations to be performed per reservoir process and resolution requirements in terms of grid cells employed. Thus the need for accurate and efficient numerical methods in reservoir simulation is paramount. Many existing commercial simulators still use low order methods and while the efficiency of a low order scheme can be improved with grid adaptivity [1, 3–11], a high density of elements is still required in the locally refined regions.

For many problems, regions of interest with large flow gradients occupy only a small percentage of the flow domain at any given time, and therefore the ability to perform dynamic local mesh refinement in regions of interest is highly desirable. Benefits of increased accuracy and reduced computational cost have been achieved by coupling dynamic multilevel grid adaptivity with a higher order accurate space–time monotonicity preserving Godunov scheme both for uniform homogeneous and heterogeneous permeability fields, respectively [12, 13]. For a given level of grid refinement, the adaptive high order scheme is up to a factor of four times faster than the first-order single point upstream weighting scheme employing a uniform grid of the same level, while producing results of far superior quality [14].

A cell centered finite volume discretization of the flow equations is employed in constructing the adaptive higher order scheme. In a cell centered formulation the flow domain is represented by a grid of quadrilateral cells. All rock and flow variables including saturations, concentrations, and pressures are defined at the cell centers and the flow equations are integrated over each cell using the Gauss flux theorem. The discrete cell face fluxes are then constructed from approximations based on the cell centered variables. Details of the hyperbolic scheme are given in [14]. The cell centered pressure equation approximation is described below. Use of such a discretization for the pressure equation results in a local leading truncation error of $O(1/h)$ when applied to h-adaptive grids with local refinement [1–3].

An analysis of the scheme on large aspect ratio grids reveals that the error coefficient is proportional to grid interface ratio, grid aspect ratio, permeability, and the pressure gradient acting tangentially to the grid interface, bordering differing levels of grid refinement. Results are presented which show that on small aspect ratio grids the $O(1/h)$ error can have a small or negligible effect upon the solutions [15]. Provided that tangential flow gradients

0021-9991/96 $18.00

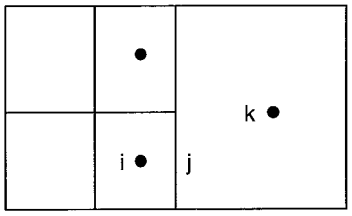

FIG. 1. Adaptive interface (ratio = 2).

remain sufficiently small, convergence is expected [3]. However, for flow in a vertical cross section it has been shown that the local error can have a significant impact on the solution [2]. Computations presented here involve flow with significant gradients tangential to h-adaptive grid interfaces and the effect of the leading error is clearly demonstrated for large aspect ratio grids.

In this paper a new flux continuous correction [15] is presented, together with an improved version of a previously proposed explicit correction [1, 2]. While both corrections eliminate the leading error, the new correction exhibits the best rates of computed convergence. The comparative simplicity of the new scheme facilitates a fully implicit implementation, whereas the more complicated correction scheme is implemented explicitly.

The new (finite volume) scheme is specifically designed to remove the leading error, ensure flux continuity, and maintain local mass conservation. Other properties include: a symmetric positive definite matrix for discrete anisotropic coefficients, diagonally dominant for discrete locally isotropic coefficients, convergence to $O(h)$ is shown for a local refinement interface, and support of the standard approximation is retained, ensuring that the original matrix structure is unchanged. Effort in implementation is minimal, with only a change in coefficients of the standard scheme at the interfaces. The merits of this approximation are weighed against those of the standard approximation and the improved explicit correction scheme [2]. Computed velocity and pressure convergence rates are shown for all three schemes. The effect of each discretisation is also illustrated for multilevel dynamically adaptive two phase flow simulations.

2. THE DISCRETE PRESSURE EQUATION WITH LOCAL GRID REFINEMENT

Adaptivity

Key ingredients of the adaptive method are its ability to refine an element, which consists of subdivision of a quadrilateral cell (father) into four cells (sons), and unrefine an element, i.e., remove the four sons and replace them by the father [16]. Here multilevel refinement is performed such that the maximum number of cells adjacent to a given element face is limited to two (Fig. 1) (i.e., the grid interface ratio constraint $G_r = 2$), ensuring grid regularity with respect to discretization error which is discussed below. Adaptivity and criteria for deciding when to refine/unrefine an element are discussed in [2, 12–14].

Classical Finite Volume Discretization of the Pressure Equation

In this paper the focus is on the discretization of the diagonal anisotropic pressure equation

$$-\left(\frac{\partial}{\partial x}k_x\frac{\partial p}{\partial x}+\frac{\partial}{\partial y}k_y\frac{\partial p}{\partial y}\right)=q, \tag{2.1}$$

where $\mathbf{k} = (k_x(x, y), k_y(x, y))$ is a diagonal tensor. The domain Ω is partitioned into a grid of quadrilateral cells Ω_i and a discrete permeability k_i and pressure p_i is associated with the center of each cell. A cell centered approximation of the pressure equation for quadrilateral grids with local refinement is derived via an application of the Gauss flux theorem to Eq. (2) over each cell Ω_i to obtain

$$-\sum_j \mathbf{n}_j \cdot k_j \nabla p \Delta s_j = q_i A_i, \tag{2.2}$$

where $q_i A_i$ is the sum of the mass flow rate and integral of the gravity term, A_i is the area of the ith cell, j is the local number of cell faces and has a maximum value that varies between 4 and 8 on adaptive grids, $\mathbf{n}_j$ and Δs_j are the outward unit normal vector and length of the jth cell face, respectively, k_j is the cell face coefficient (transmissibility) which must be defined such that pressure and flux are continuous (see Section 4). Approximation of the jth face normal flow gradient by a classical cell centered difference results in

$$\mathbf{n}_j \cdot \mathbf{k}\nabla p = k_j(p_k - p_i)/\Delta n_{ik}, \tag{2.3}$$

where p_k is the pressure at the center of the kth neighbouring cell and Δn_{ik} is the distance between the ith and kth cell centers in the direction normal to face j, Fig. 1. The integral approximation (2.2) ensures local conservation, diagonal dominance, and a symmetric positive definite matrix for any locally refined quadrilateral grid. We note in passing that if the discrete equation is not integrated so that, instead of (2.2), we solve for p directly from

$$\frac{-\sum_j \mathbf{n}_j \cdot k_j \nabla p \Delta s_j}{A_i} = q_i$$

then while local conservation is maintained the discrete matrix would only be symmetric in shape and nonsymmetric in coefficients even for a regular nonuniform grid due to the variation in cell areas A_i.

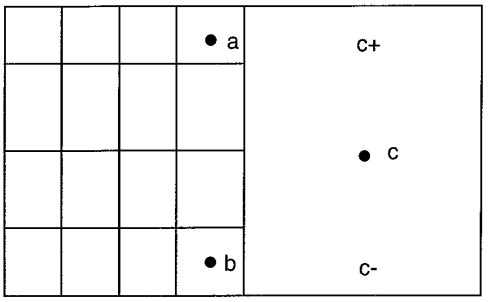

FIG. 2. Interface: Pressure locations for orthogonal flux.

Error Analysis of the Classical Finite Volume Scheme

Approximation of a normal derivative by the standard difference of cell centered quantities at an adaptive grid interface can inevitably lead to a severe error, since a line joining coarse and fine adjacent cell centers across the interface is strictly nonorthogonal to the interface and the resulting approximate derivative is skew to the fine-cell (Fig. 2). A summary of the truncation error analysis [2] of the above scheme at an adaptive grid interface follows.

We consider a locally refined grid with an interface tangential to the y direction having coarse and fine cell dimensions of (H_x, H_y) and (h_x, h_y), respectively. The coarse and fine cell dimensions are related through $(h_x, h_y) = (H_x/G_r, H_y/G_r)$, where G_r is an arbitrary integer interface ratio in this analysis (e.g., $G_r = 4$ in Fig. 2) and the grid aspect ratio $A_r = h_y/h_x$ (Fig. 2). The global indices of the fine cells and coarse cell which enter this analysis are denoted by a, b, and c (Fig. 2). Appropriate normal derivative approximations at the faces of cells a and b of Fig. 2 are given by

$$(p_{c+} - p_a)/\Delta x \tag{2.4a}$$

$$(p_{c-} - p_b)/\Delta x, \tag{2.4b}$$

where p_{c+} and p_{c-} are the pressures at a distance $H_y(1 - 1/G_r)/2$ above and below coarse cell center c and $\Delta x = H_x(1 + 1/G_r)/2$. By Eq. (2.3) the standard difference approximations at the faces of cells a and b are $(p_c - p_a)/\Delta x$ and $(p_c - p_b)/\Delta x$. Subtracting these respective differences from Eq. (2.4) reveals that the respective errors in pressure gradient at the faces of cells a and b due to nonorthogonality are given by

$$(p_c\pm - p_c)/\Delta x. \tag{2.5}$$

In calculating the leading truncation errors in the pressure equation discretisations at cells a, b, Eq. (2.5) contributes local velocity errors of

$$\pm A_r k_x \frac{G_r - 1}{G_r + 1}\frac{\partial p}{\partial y} \tag{2.6}$$

which in turn contribute leading discretisation errors of

$$\pm k_x \frac{A_r G_r (G_r - 1)}{H_x (G_r + 1)}\frac{\partial p}{\partial y} + O(1), \tag{2.7}$$

where $\partial p/\partial y$ is the pressure gradient tangential to the interface. Alternatively the errors at an interface tangential to the x axis are obtained from (2.7) by interchanging x and y to give

$$\pm k_y \frac{A_r G_r (G_r - 1)}{H_y (G_r + 1)}\frac{\partial p}{\partial x} + O(1), \tag{2.8}$$

where now $A_r = h_x/h_y$.

The errors are proportional to the local tangential flow gradient, both of the respective grid interface and aspect ratios and permeability. For the h-adaptive grid data structure used here $G_r = 2$, which minimizes the error in the standard discretization with respect to interface ratio. Despite the $O(1/h)$ error, results displayed below show that this scheme can still be effective for small aspect ratio or even larger A_r, provided that the corresponding directional permeability has an appropriately reduced variation. However, in general, for larger variations in grid aspect ratio and/or permeability a correction is essential; cf. Section 6.

3. EXPLICIT ERROR CORRECTION AT AN ADAPTIVE GRID INTERFACE

Error correction by polynomial interpolation of the pressure between neighboring cells tangential to an h-grid interface is proposed in [1], for a fixed grid with a single level of local refinement. Referring to Fig. 3 for the case $G_r = 2$, replacement of $(p_c - p_b)/\Delta x$ by

$$(p_{c-} - p_b)/\Delta x \tag{3.1}$$

(where $p_{c\pm}$ are the interpolated pressures) reduces the velocity error τ_{vel} from $O(1)$ to $O(h)$, where (due to the interpolant error)

$$\tau^{\pm}_{\text{vel}} = \pm h_y A_r p_{yy} k_x/4 + O(h_y^2) \tag{3.2}$$

and the local truncation error is reduced from $O(1/h)$ to $O(1)$ at cells a and b, respectively. This correction procedure has been generalized to dynamic grids with n levels of refinement [2]. If neighboring cells share the same value of permeability, then use of the second-order linear inter-

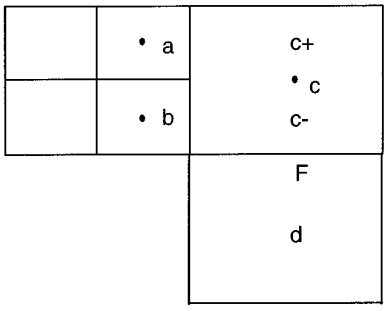

FIG. 3. Correction by interpolation.

polation between the cell centered pressures following [1] is a valid approximation. For the case of Fig. 3, this results in

$$p_{c-} = (3p_c + p_d)/4. \tag{3.3}$$

However, for a generally varying permeability field p_{c-} must be given by Eq. (4.4) as explained in the next section.

A fully implicit correction results in conditional diagonal dominance and a loss of symmetry in the pressure matrix, together with increased complexity in the connectivity. Asymmetry is demonstrated by referring to Fig. 3; the discrete pressure equation for cell b involves data from cell d, whereas the converse is not true.

Alternatively an explicit correction can be incorporated into the standard scheme by writing the correct normal gradient as the sum of the standard cell centered difference and a tangential correction,

$$(p_{c-} - p_b)/\Delta x = (p_c - p_b + p_{c-} - p_c)/\Delta x, \tag{3.4}$$

which can be approximated in time as

$$(p_c^{n+1} - p_b^{n+1} + p_{c-}^n - p_c^n)/\Delta x \tag{3.5}$$

and using Eq. (3.5) in the definition of the total velocity at the interface maintains local conservation and leaves the pressure matrix unchanged, with the correction added to the right-hand side of the standard discrete pressure equation. The method is implemented as a deferred correction technique, with each dynamic change in the grid; the standard uncorrected pressure equation is solved to provide an initial ''predicted'' pressure field; then a second iteration is performed using the corrected pressure equation via Eq. (3.5).

A significant improvement in results is obtained with this approach. However, while this correction removes the $O(1/h)$ error leaving an $O(1)$ local spatial truncation error, time lagging introduces an additional $O(1)$ error.

4. FLUX CONTINUOUS APPROXIMATION

Since flux and pressure are continuous and the coefficient can be discontinuous, the pressure field can have discontinuous gradients at a cell edge. Therefore polynomial intepolation is not strictly valid across neighboring cell faces. Continuous pressure and flux are built into the discrete cell centered approximation as follows: A mean value of pressure p_f is introduced at a cell face between neighboring cells (Fig. 4) and is used with adjacent cell centered pressures, to construct a continous piecewise linear approximation to pressure in each cell. Equating the resulting one-sided flux approximations,

$$k_r \frac{p_r - p_f}{\Delta x_r} = k_l \frac{p_f - p_l}{\Delta x_l} \tag{4.1}$$

ensures flux continuity to $O(h)$. From Eq. (4.1) the pressure and flux at the cell face are given by

$$p_f = (p_l k_l/\Delta x_l + p_r k_r/\Delta x_r)/(k_l/\Delta x_l + k_r/\Delta x_r) \tag{4.2}$$

$$f = -\frac{2k_r k_l (p_r - p_l)}{(k_r \Delta x_l + k_l \Delta x_r)}. \tag{4.3}$$

The coefficient in Eq. (4.3) is the harmonic mean of permeabilities commonly used in reservoir simulation [17]. Returning to the correction of Section 3, for a variable permeability field, a cell face value of pressure can be defined at F in Fig. 3 using Eq. (4.2). Interpolation can then be performed between the pressure at the cell center c and cell face F, respectively. The resulting interpolant corresponding to Eq. (3.3) is

$$p_{c-} = ((2k_c + k_d)p_c + k_d p_d)/2(k_c + k_d). \tag{4.4}$$

Use of Eq. (3.3) results in a conditionally diagonally dominant matrix for implicit implementation, whereas use of Eq. (4.4) results in unconditional diagonal dominance for locally isotropic coefficients (proof in Appendix 1).

5. FLUX CONTINUOUS CORRECTION AT AN ADAPTIVE GRID INTERFACE

A new approximation of the flux at an adaptive grid interface is introduced which gives rise to a pressure equa-

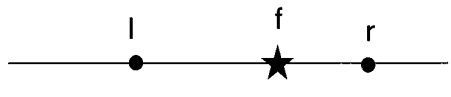

FIG. 4. Flux continuity between cells in 1D (f is at the cell face).

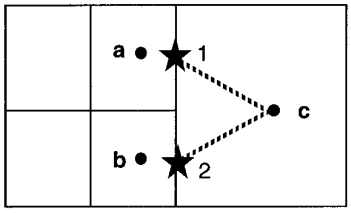

FIG. 5. Flux continuity at an adaptive interface (ratio = 2).

tion discretization with the following properties:

(1) Continuous flux and pressure at an *h*-adaptive interface

(2) Symmetric positive definite discrete matrix

(3) Diagonally dominant discrete matrix for locally isotropic coefficients

(4) Supra-convergence to $O(h)$ is demonstrated for an adaptive interface

(5) Retains local conservation and same support and matrix structure as the standard finite volume scheme

(6) Fully implicit implementation

(7) Generalisation to arbitrary grid interface ratio refinement.

The aim here is to construct a flux which is orthogonal to the interface while maintaining a purely local approximation, thereby avoiding the complexities which arise with the tangential interpolation of Section 3. A mean flux is constructed at the midpoint face between two neighboring cells of the same level of refinement at an *h*-adaptive grid interface. For illustration assume the coefficient takes the same value in all three cells forming the interface (Fig. 5); then a mean normal interface velocity can be defined by

$$V|_{\text{face}} = -\frac{2}{3h}k\left(p_c - \frac{(p_a + p_b)}{2}\right). \tag{5.1}$$

This flux is constant over faces 1 and 2 (Fig. 5) and has the advantages of both, removing the $O(1)$ error in velocity (Appendix 2) while retaining local conservation and support of the standard finite volume scheme.

Flux and Pressure Continuity

For generally varying pressure equation coefficients the flux is constructed such that both pressure and flux are continuous across faces 1 and 2 (Fig. 5). These constraints are achieved by introducing mean pressures at 1 and 2, then applying a piecewise linear approximation to pressure over the resulting triangle 1,2,*c* (Fig. 5). The fluxes on the left-hand side of faces 1 and 2 are equated to the flux on the right-hand side resulting in two equations for the two mean face pressures p_1 and p_2, respectively,

$$\begin{aligned} k_{x_a}\frac{(p_1 - p_a)}{h_x/2} &= k_{x_c}\frac{(p_c - (p_1 + p_2)/2)}{h_x} \\ k_{x_b}\frac{(p_2 - p_b)}{h_x/2} &= k_{x_c}\frac{(p_c - (p_1 + p_2)/2)}{h_x}, \end{aligned} \tag{5.2}$$

where (h_x, h_y) are the fine cell dimensions and k_{x_a} is the horizontal permeability of cell a. This procedure is a generalization at an *h*-adaptive interface of the 1D flux continuous derivation of Section 4. Eliminating p_1 and p_2 in terms of p_a, p_b, and p_c yields a flux

$$f = -4\frac{h_y}{h_x}\frac{k_{x_a}k_{x_b}k_{x_c}(p_c - (p_a + p_b)/2)}{(4k_{x_b}k_{x_c} + k_{x_a}(k_{x_b} + k_{x_c}))}. \tag{5.3}$$

Properties (2) to (5) are illustrated by considering matrix contributions at the interface. As in Section 2 the discrete scheme is constructed in integral form. Away from the interface we have the usual scheme and therefore those matrix components are symmetric, positive semi-definite, and diagonally dominant.

The flux contributions to cells a, b, and c from the adjacent interface cells (b and c for a, a and c for b, and a and b for c) (Fig. 5) are respectively

$$-w_{abc}(p_c - (p_a + p_b)/2) + w_{ab}(p_a - p_b) \tag{5.4a}$$

$$-w_{abc}(p_c - (p_a + p_b)/2) - w_{ab}(p_a - p_b) \tag{5.4b}$$

$$2w_{abc}(p_c - (p_a + p_b)/2), \tag{5.4c}$$

where

$$w_{abc} = 4\frac{h_y}{h_x}\frac{k_{x_a}k_{x_b}k_{x_c}}{(4k_{x_b}k_{x_c} + k_{x_a}(k_{x_b} + k_{x_c}))} \tag{5.5a}$$

and

$$w_{ab} = 2\frac{h_x}{h_y}\frac{k_{y_a}k_{y_b}}{(k_{y_a} + k_{y_b})} \tag{5.5b}$$

and the factor of 2 appears in the coefficient of flux Eq. (5.4c) since the face of the coarse cell is of length $2h_y$.

Local Conservation

The new interface approximation has been specifically constructed to remove the $O(1)$ velocity error and ensure local conservation (i.e., a finite volume scheme is retained) which is easily demonstrated by inspection of Eq. (5.4); referring to Fig. 5 both the addition of the flux components

between cells a and b tangential to the interface and flux components between cells a, b, and c normal to the interface sum to zero as required.

Symmetric Matrix

Assembling interface contributions of matrix $\mathbf{M}$ we find that for row a,

$$M_{aa} = \frac{w_{abc}}{2} + w_{ab}, \quad M_{ac} = -w_{abc}, \quad M_{ab} = \frac{w_{abc}}{2} - w_{ab}; \tag{5.6a}$$

for row b,

$$M_{bb} = \frac{w_{abc}}{2} + w_{ab}, \quad M_{bc} = -w_{abc}, \quad M_{ba} = \frac{w_{abc}}{2} - w_{ab}; \tag{5.6b}$$

and for row c,

$$M_{cc} = 2w_{abc}, \quad M_{ca} = -w_{abc}, \quad M_{cb} = -w_{abc}; \tag{5.6c}$$

therefore

$$M_{ab} = M_{ba}, \quad M_{ca} = M_{ac}, \quad M_{cb} = M_{bc}$$

and, thus, the matrix is symmetric.

Positive Definite Matrix

Consider the contributions from the interface to the energy-inner product $\mathbf{P}^{\mathrm{T}}\mathbf{MP}$, where $\mathbf{P}$ is an arbitrary vector. Assembling the appropriate contributions from cells c, a, and b, we obtain

$$\begin{aligned} &2p_c w_{abc}(p_c - (p_a + p_b)/2) - p_a(w_{abc}(p_c - (p_a + p_b)/2) \\ &\qquad - w_{ab}(p_a - p_b)) \\ &\qquad - p_b(w_{abc}(p_c - (p_a + p_b)/2) + w_{ab}(p_a - p_b)) \\ &\quad = 2w_{abc}(p_c - (p_a + p_b)/2)^2 + w_{ab}(p_a - p_b)^2 \end{aligned} \tag{5.7}$$

which is bounded below by zero. Use of the Dirichlet condition ensures $\mathbf{P}^{\mathrm{T}}\mathbf{MP} > 0$ for any $\mathbf{P}$. We conclude that the matrix is symmetric positive definite, which guarantees existence and uniqueness of the solution for general discrete coefficients and matrix inversion by standard solvers.

Positive Diagonal Dominance

Again it is only necessary to consider matrix elements for the interface. Diagonal dominance with positive diagonal and negative (or zero) off-diagonal coefficients (and therefore a discrete maximum principle) follows if

$$M_{aa} \geq |M_{ab}| + |M_{ac}|$$

and from Eq. (5.6a), (5.6b) this is true if

$$w_{ab} \geq \frac{w_{abc}}{2}, \tag{5.8}$$

using the definitions in Eq. (5.5) it follows that Eq. (5.8) is satisfied if

$$\frac{h_x}{h_y}\frac{k_{y_a}k_{y_b}}{(k_{y_a} + k_{y_b})} \geq \frac{h_y}{h_x}\frac{k_{x_a}k_{x_b}k_{x_c}}{(4k_{x_b}k_{x_c} + k_{x_a}(k_{x_b} + k_{x_c}))}. \tag{5.9}$$

Strict inequality holds in Eq. (5.9) if

$$k_{y_a} \geq A_r^2 k_{x_a}, \quad k_{y_b} \geq A_r^2 k_{x_b} \tag{5.10}$$

in particular for equality in Eq. (5.10) with unit aspect ratio, it follows that the matrix is diagonally dominant subject to locally discrete isotropic spatially varying coefficients. The condition of Eq. (5.8) ensures that the new scheme has an M matrix, which is also important in the case of solvers based on multigrid [18].

Supra-Convergence

When the solution error converges faster than the discretization error the scheme is supra-convergent [19]. Supra-convergence of the cell centered scheme on a regular nonuniform grid without local refinement has been proven via the mixed finite element formulation [20] and by construction of a second-order grid function [21].

Supra-convergence at an adaptive grid interface (shown in Appendix 2) is demonstrated by transforming the new nonstandard interface operators acting on cell centered values into classical five point operators acting on mean values. Convergence with respect to mean values and thus cell centered values follows.

The leading truncation error in velocity at the center of the fine cell faces 1 and 2 (Fig. 5) is shown below (Appendix 2) to be of $O(h)$ compared to $O(1)$ for the standard scheme of Section 2 (cf. Eq. (2.6)). The new flux continuous scheme eliminates the $O(1/h)$ discretization error leaving a leading local spatial truncation error of $O(1)$ in the pressure equation discretization at the interface. Supra-convergence to $O(h)$ is demonstrated in Appendix A2 for an adaptive grid interface.

Scheme Support

Definition of the new correction relies on nearest neighbours (Eq. (5.4)); hence, support of the scheme is unchanged. As a consequence of properties (2) and (6), any matrix solver applicable to the standard finite volume scheme is applicable to the new correction scheme so that implicit inversion is ensured.

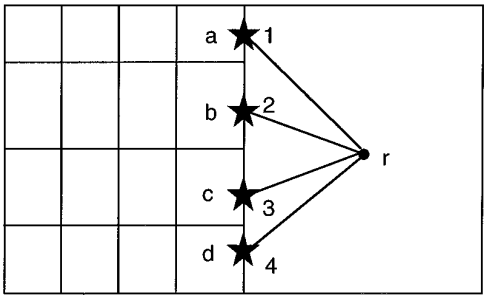

FIG. 6. Flux continuity at an adaptive interface (arbitrary ratio).

Alternative Procedure

Returning to Eqs. (5.2) there is an alternative way to proceed; the interface (mean) pressures can be regarded as additional degrees of freedom and the flux continuity equations can be added to the system of discrete equations to be solved for the pressures (a similar approach has been taken for disjoint grids at faults [22]). However, while this procedure also increases accuracy and proves to be effective for removing the interface error, the number of unknowns increases by Gr per *local* interface (of which there are many in a typical adaptive grid, here Gr = 2 per local interface in 2D). This hybrid approach adds further complexity to the data structure in order to store cell face *and* cell centered pressures. Further examination of this procedure and further comparisons will be reported in [23].

Extension to Grids of Larger Interface Ratio

For adaptive grids of arbitrary grid interface ratio G_r, a flux continuous approximation can be constructed by introducing G_r interface pressures and $G_r - 1$ triangles each connected to the coarse grid cell center as in the example of Fig. 6. Piecewise constant fluxes corresponding to appropriate adjacent triangles are equated to their fine grid flux counterparts on the left-hand side of the interface as illustrated in Appendix A3.

Adaptive Pressure Matrix Inversion

The conjugate gradient method with diagonal preconditioning is used to invert the symmetric pressure matrix in this work. The explicit nature of the conjugate gradient method is exploited, since the method only involves the pressure matrix elements through explicit operations of the discretization operator on residual vectors, it is easily incorporated into an adaptive code where the discrete operator is already assembled. This approach avoids matrix storage issues, requires no knowledge of the matrix band structure and will generalize to any solver based on explicit matrix multiply operations.

6. FLOW EQUATIONS AND RESULTS

In the first subsection 6a computed convergence rates for single phase homogeneous and heterogeneous examples are shown for the three types of pressure equation discretisation presented in this paper.

In the second subsection 6b an example reservoir simulation equation set and problems are presented, together with the solutions computed by the standard *uncorrected* and *newly corrected* complete adaptive higher order hyperbolic elliptic method. The results in this section show when the uncorrected scheme can be of use and when a correction is required.

6a. Convergence Rates Corresponding to the Pressure Equation Discrete Operators

Convergence of the concentration equations on grids with local refinement is a separate issue beyond the scope of this paper and will be considered in a future paper [23].

Convergence rates are presented for the velocities and pressures obtained using the three types of discretization discussed above on grids with local refinement. In order to see as clearly as possible the effects of the discrete operators under identical conditions, convergence rates are studied for the pressure equation alone; i.e., a steady state problem is solved in isolation from the concentration

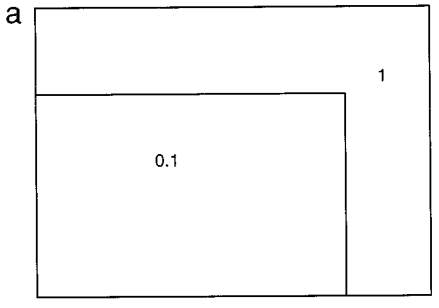

Permeability Map Kx (Homogeneous)

b

0.81	0.97	0.75	0.76
0.16	0.55	0.3	0.26
0.67	0.52	0.022	3x10-5
0.006	0.37	0.41	0.83

Kx Permeability Map (Heterogeneous)

Ky=A*Kx 8 < A < 16

FIG. 7. *Kx* permeability maps for convergence tests.

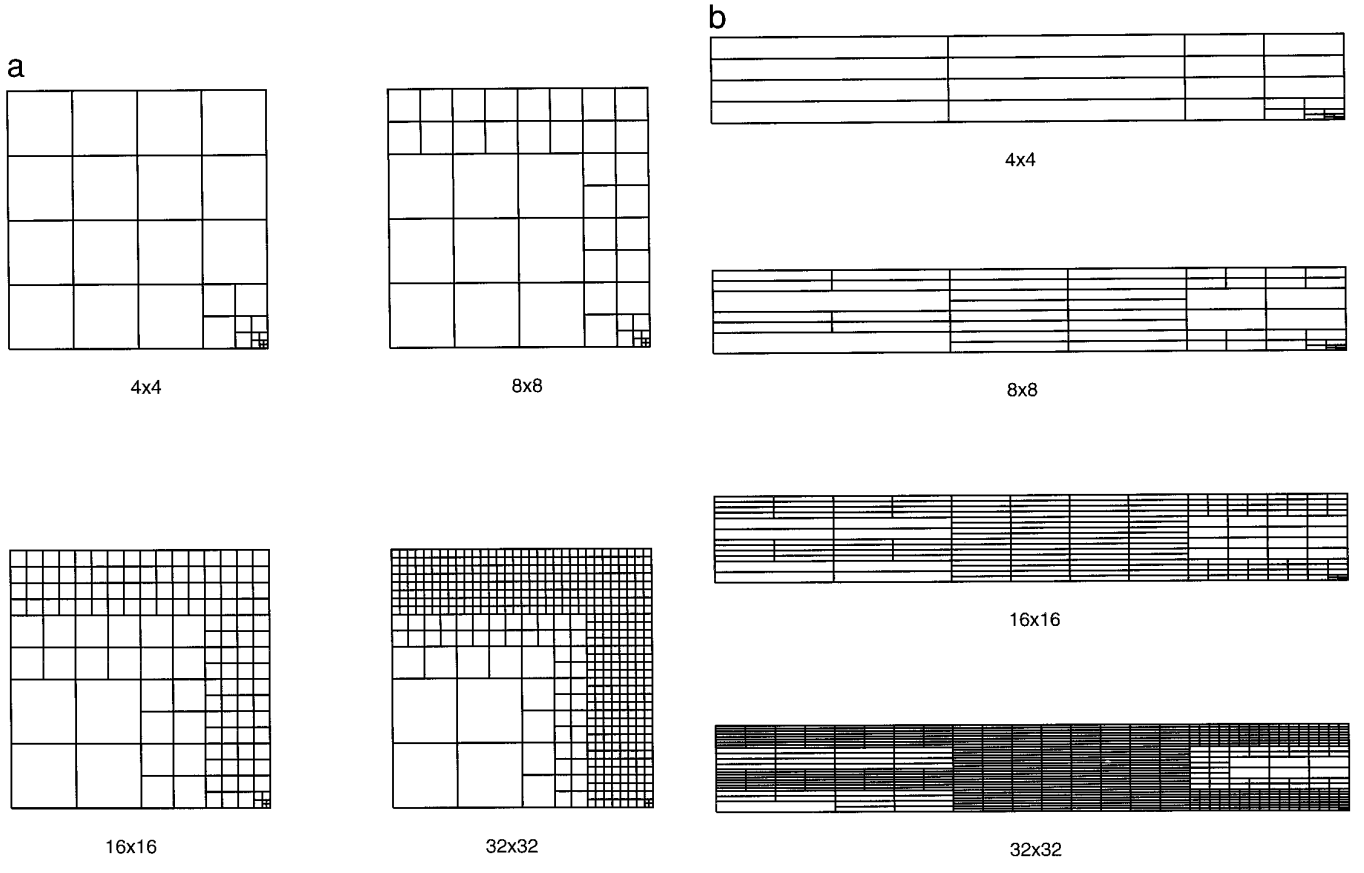

FIG. 8. a. Homogeneous partial grid sequence; b. Heterogeneous partial grid sequence.

equations. A sequence of static locally refined grids is used for convergence tests. For a given coarse permeability map each grid is locally refined according to the local variation in permeability and the sequence of grids is defined by allowing each new grid to have one extra level of local refinement compared to its predecessor.

Solid wall (zero flow) conditions are imposed on all boundaries except the top left-hand cell where flux (or flow rate) is specified and the bottom right-hand cell where a Dirichlet condition is imposed in order to allow out flow. The latter cell containing the (sink) Dirichlet condition is always refined to the maximum level considered in order to remove outflow boundary condition effects from the local refinement study.

Two types of permeability variation are considered; homogeneous and heterogeneous. They are shown in Fig. 7 (the permeability anisotropy ratio denoted by $k_r = k_y/k_x$ is defined below for each case) and the sequence of locally refined grids for (four of the five levels) levels 4 to 32 are shown in Figs. 8a and 8b, respectively. In each case the permeability map is used to define the permeabilities on a 4×4 coarse cell grid. These values are then used to define finer grid permeabilities, thus ensuring that the problem is identical with respect to each grid level used for testing convergence of the scheme. In each case the uniform grid solution is computed on a 64×64 grid and the log of the residual of the difference between the locally refined grid solutions (4×4 to 64×64) and the 64×64 uniform fine grid solution is plotted against log N (where $4 \leq N \leq 64$) to demonstrate convergence rates. The convergence rates of all schemes in L_1, L_2, and L_∞ lead to the same conclusions in terms of scheme classification; however, the L_1 convergence rates are the most uniform and these are presented.

Homogeneous, $A_r = 1$, $K_r = 1$

Convergence rates for velocity show that for a unit aspect ratio grid with isotropic permeability all schemes produce approximately $O(h)$ convergent velocities, although the corrected schemes do show a slight improvement in convergence (Fig. 9). It is interesting to note, particularly for the coarser grid levels, that the velocity errors for all schemes are almost equal, showing that the correction has little effect which might be expected as the leading error coefficient in Eq. (2.8) is minimised with $K_rA_r = 1$. The pressure

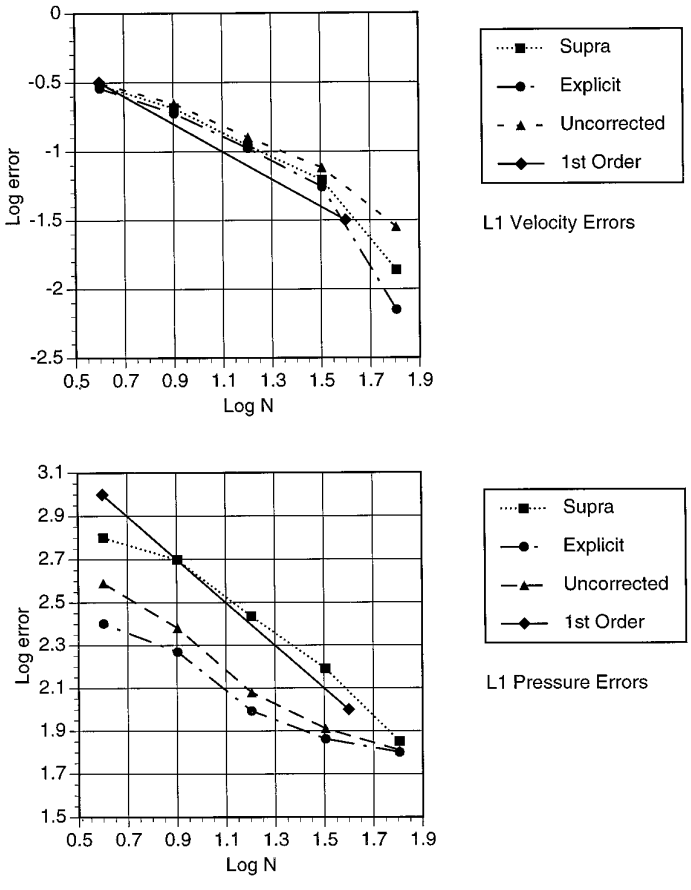

FIG. 9. Velocity pressure convergence: Unit grid aspect ratio, isotropic permeability.

errors are greater than the velocity errors in all cases; however, the new scheme clearly shows $O(h)$ convergence.

Homogeneous, $A_r = 8$, $K_r = 1/8$

For a grid aspect ratio $A_r = 8$ and permeability ratio of 1/8 the standard scheme again exhibits convergence, slightly less than $O(h)$ while both corrections show velocity convergence slightly better than $O(h)$ (Fig. 10). The new scheme again shows $O(h)$ pressure convergence. The error coefficient (2.8) is minimized as in the unit aspect ratio case with $K_r A_r = 1$ and the behavior observed in both of these cases is consistent with the full simulation problem described below.

Homogeneous, $A_r = 8$, $K_r = 1$

For a grid aspect ratio $A_r = 8$ and isotropic permeability the standard uncorrected scheme shows a deterioration in convergence in pressure and velocity (Fig. 11) (the leading error increases by a factor of 8 (cf. Eq. (2.8)), while the corrected schemes maintain convergence. The explicit correction is nearly $O(h)$ and the new scheme is $O(h)$ in pressure and velocity.

Heterogeneous, $4 \le A_r \le 12$, $K_r \ge 8$

In the heterogeneous case the difference in performance of the schemes increases. Referring to Fig. 12, the explicit correction still indicates convergence, albeit somewhat less than $O(h)$. The new scheme still firmly shows convergence, now nearly $O(h)$ for velocity and pressure, while the uncorrected scheme fails to indicate convergence in velocity and diverges in pressure. The convergence rates presented demonstrate supra-convergence of the corrected flux approximations. The new scheme displays the best overall rates of convergence in pressure and velocity in all cases.

The analysis in this paper shows that the new scheme is supra-convergent. The formal discrete truncation error of the corrected scheme is $O(1)$ while the solution error and velocity error at a single interface is shown to be at most $O(h)$. Convergence rates are presented for a variety of problems and convergence is always obtained by the new scheme.

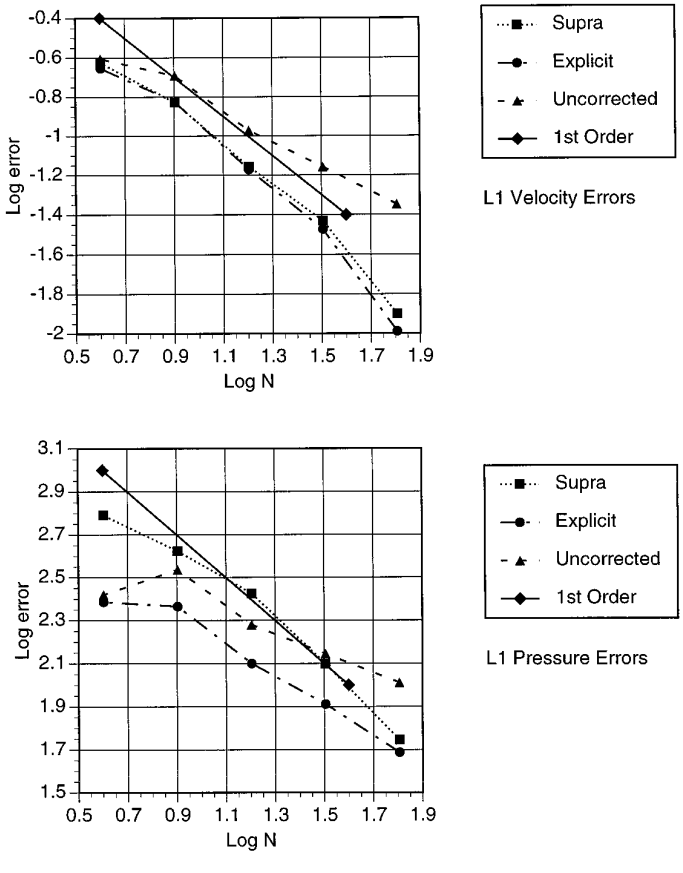

FIG. 10. Velocity pressure convergence: Grid aspect ratio = 8; Anisotropic permeability ratio = 1/8.

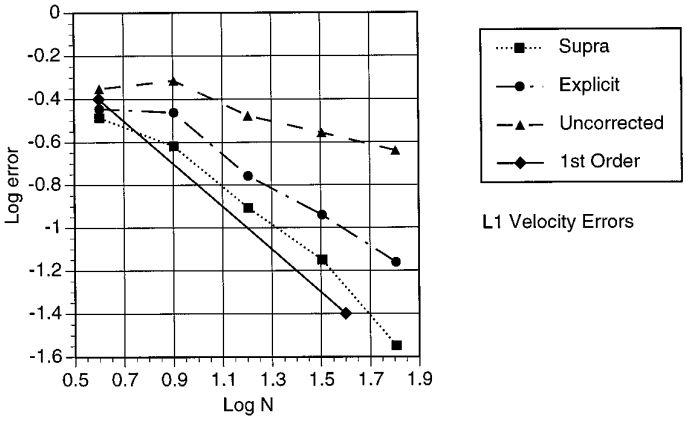

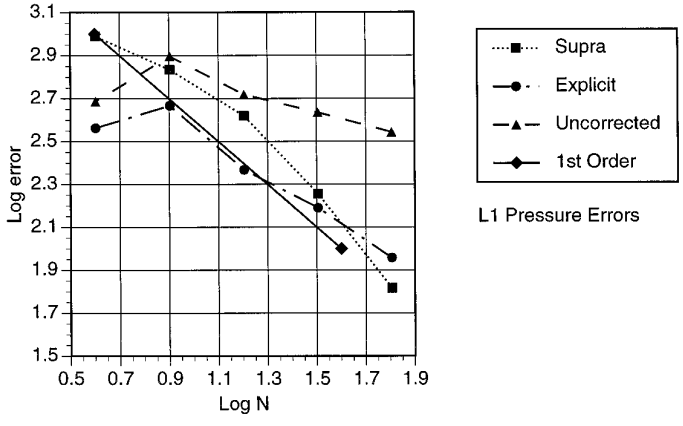

FIG. 11. Velocity pressure convergence: Grid aspect ratio = 8; Isotropic permeability.

6b. Practical Effects of the Interface Error

The practical effects of the interface errors discussed in the above sections are clearly demonstrated in the following examples. The reservoir simulation equation set considered here is stated below. A detailed description of the derivation can be found in [17], for example. The flow is assumed to be incompressible; capillary pressure and dispersion are neglected; porosity and total permeability are held constant. The flow equations studied here are

$$\partial s_j/\partial t + \nabla \cdot \mathbf{v}_j = q_j \tag{6.1a}$$

$$\nabla \cdot \mathbf{V}_t = q \tag{6.1b}$$

$$\sum_{j=1}^{2} s_j = 1,$$

where s_j and $\mathbf{v}_j$ denote the phase saturations and velocities, respectively; $\mathbf{V}_t = \mathbf{v}_1 + \mathbf{v}_2$ is the total velocity; $\mathbf{v}_1$ and $\mathbf{v}_2$ are gas and oil phase velocities; and q is the sum of the corresponding source terms. The jth phase velocity is a function of pressure p and is given by

$$\mathbf{v}_j = -\mathbf{k}\lambda_j(\nabla p + \rho_j g \nabla h), \tag{6.2}$$

where $\lambda_j = k_{rj}/\mu_j$ is the phase mobility; k_{rj}, ρ_j, and μ_j are the respective relative permeability, density, and viscosity; $\mathbf{k}$ is the permeability tensor; g is the acceleration due to gravity; and h is the height. We assume k_{rj} is quadratic in saturation s_j and viscosity is constant. The flux is expressed in terms of the total velocity by eliminating the pressure gradient from Eq. (6.2) to give

$$\mathbf{v}_j = f_j(\mathbf{V}_t + \lambda_k g \nabla h(\rho_2 - \rho_1)),$$

where $f_j = \lambda_j/(\lambda_1 + \lambda_2)$ is the fractional flow and $k \neq j$. The pressure equation is defined by Eq. (6.1b) and the system equation (6.1) is solved sequentially via a total velocity formulation [14, 24]. The discrete adaptive scheme employed for the hyperbolic components of the system is described in [14].

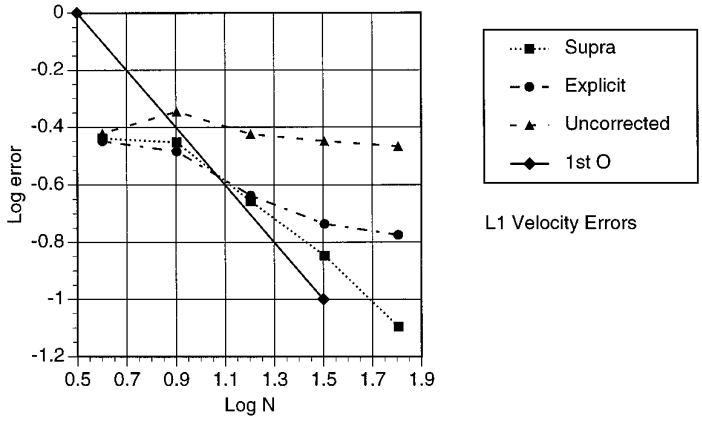

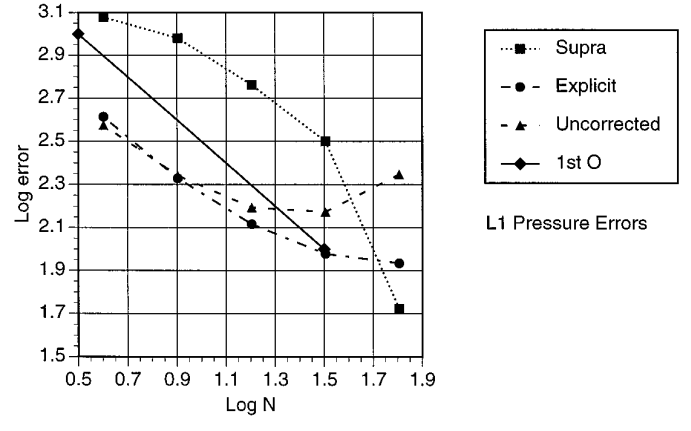

FIG. 12. Velocity pressure convergence: Heterogeneous 4 < Grid aspect ratio < 12; Anisotropic permeability ratio = 8.

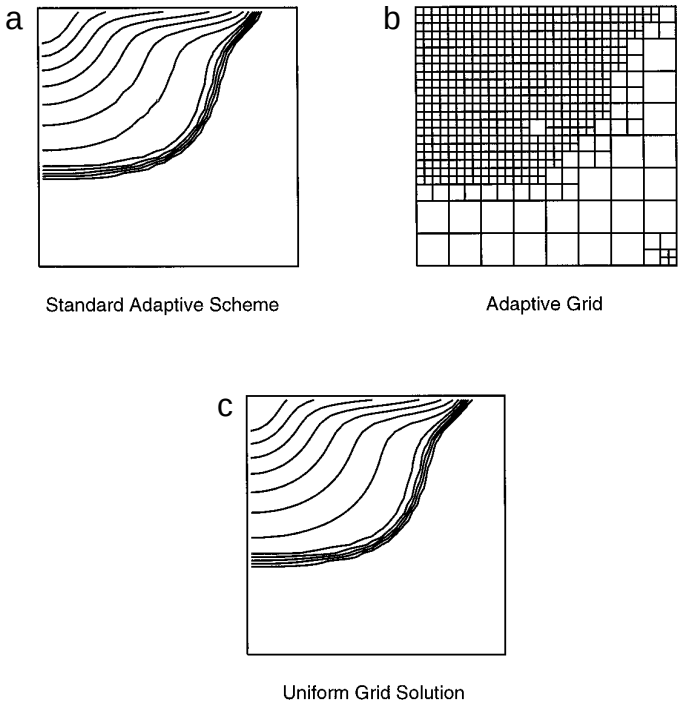

FIG. 13. Saturation field: Unit grid aspect ratio; Isotropic permeability. Dynamically adaptive simulation. Uncorrected scheme vs. Uniform grid.

The test case presented consists of a rectangular reservoir vertical cross section initially full of oil. Gas is injected in the top left-hand grid block and a production well is inserted in the bottom right grid block. The initial conditions are

$$s_1 = 0, \quad s_2 = 1$$

and solid wall boundary conditions

$$\partial p/\partial n = 0, \quad \partial s/\partial n = 0$$

apply on all walls, except at the injection and production wells, where flux and pressure are specified respectively. The *pressure* boundary conditions are identical to those in the above section 6a. The gas flows along the top of the reservoir under gravity until it reaches the right-hand solid wall, where the shock front moves towards the producer due to the high mobility of the gas (oil to gas viscosity ratio). The front breaks through at the producing well before much of the oil is recovered, giving rise to a ''cone'' at the producer.

Results are illustrated by gas saturation contours plotted at 15 uniform intervals and the output time is normalised with respect to pore volumes (pv) injected, which is the ratio of gas injected to available fluid volume of the reservoir. Sample results are shown for three variants of the problem.

Uncorrected Scheme, $A_r = 1$, $K_r = 1$

Despite the presence of an $O(1/h)$ truncation error the standard scheme of Section 2 can produce extremely good results for certain choices of grid aspect ratio and anisotropic permeability ratio.

In the first case involving a unit aspect ratio grid and isotropic permeability field excellent agreement between the adaptive scheme (with uncorrected pressure equation) (Fig. 13a) and the uniform grid scheme (Fig. 13c) is obtained.

Uncorrected Scheme, $A_r = 8$, $K_r = 1/8$

Good agreement is maintained in the second case (Fig. 14), where the grid aspect ratio $A_r = 8$ and the anisotropic permeability ratio $K_r = K_v/K_h = 1/8$. In both cases the product $K_rA_r = 1$ which minimizes the leading error coefficient of Eq. (2.8). These findings are consistent with the previous section 6a, in terms of when the uncorrected scheme exhibits good convergence behavior.

Uncorrected Scheme with Large Error, $A_r = 8$, $K_r = 1$

In a third variant of the problem the grid aspect ratio $A_r = 8$, while the permeability field is isotropic. The leading error coefficient has now increased by a factor of 8. The

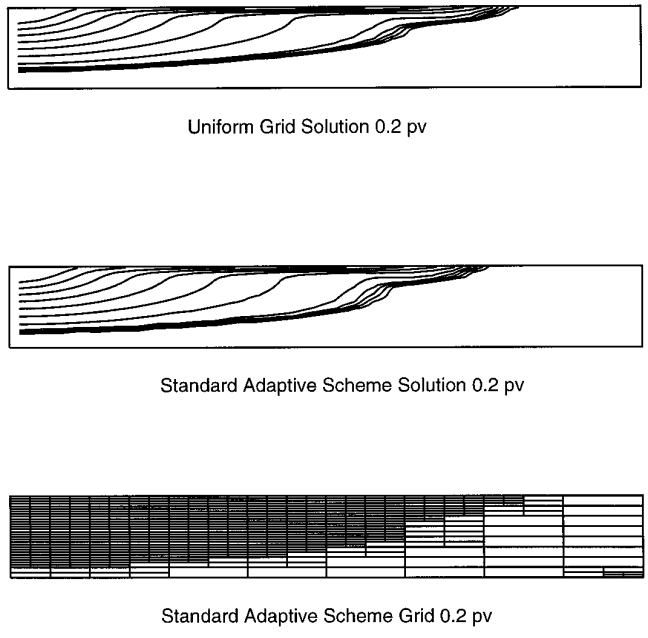

FIG. 14. Saturation field: Grid aspect ratio = 8; Anisotropic permeability ratio = 1/8. Dynamically adaptive simulation. Uncorrected scheme vs Uniform grid.

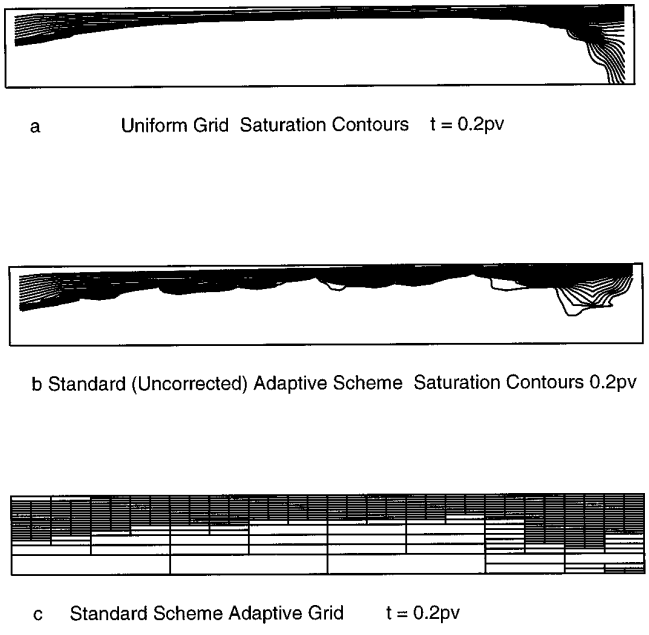

FIG. 15. Saturation field: Grid aspect ratio = 8; Isotropic permeability. Dynamically adaptive simulation. Uncorrected scheme vs Uniform grid.

solution and grid produced by the standard adaptive scheme are compared with the uniform grid solution in Fig. 15, where breakthrough of gas at the producer has just occurred at this time (15a). The interface error has a severe impact on the results with large local errors dominating the solution (15b). The error is reflected in the dynamic adaptivity where the grid is refined according to the spurious position of the distorted shock front (Fig. 15c).

Interface Corrections, $A_r = 8$, $K_r = 1$

Comparison of both correction schemes with the uniform grid scheme is shown in Fig. 16 at 0.2 pv, where flow is transient. Results from the explicit correction scheme (Section 3), show a slight time lag in solution (Fig. 16a contours near the producer), which is attributed to the deferred correction. Results of the new flux continuous scheme (supra-convergent correction of Section 5) shown in Fig. 16c are in excellent agreement with the uniform grid scheme (Fig. 16e); the corresponding adaptive grids are shown in Figs. 16b and d.

By 0.6 pv (near steady state flow and ''cone'' clearly visible) very good agreement between both of the corrected adaptive schemes and the uniform grid scheme is obtained (Fig. 17). The behavior observed is consistent with the convergence study, where for the equivalent case the standard approximation barely shows sign of convergence (Fig. 11) and for the full simulation the uncorrected scheme errors dominate the computed solution (Fig. 15b). The corrected schemes perform extremely well, both in terms of convergence and a full simulation comparison between the adaptive and uniform grid solutions.

7. CONCLUSIONS

Classical cell centered finite volume discretization of the diagonal tensor pressure equation on an h-adaptive grid results in an $O(1)$ error in velocity and an $O(1/h)$ leading truncation error in the discrete pressure equation at the grid interface dividing grids of differing levels of refinement. The error is due to representing the flux normal to the interface by a nonorthogonal difference which is inherent in the standard cell centered approximation. The error coefficient is proportional to permeability grid aspect ratio, grid interface ratio, and tangential pressure gradient. For larger grid aspect ratios and significant tangential flow gradients, the interface error has a severe impact on the results.

A new flux continuous locally conservative approximation is presented, which removes the interface error and has a symmetric positive definite matrix for general discrete

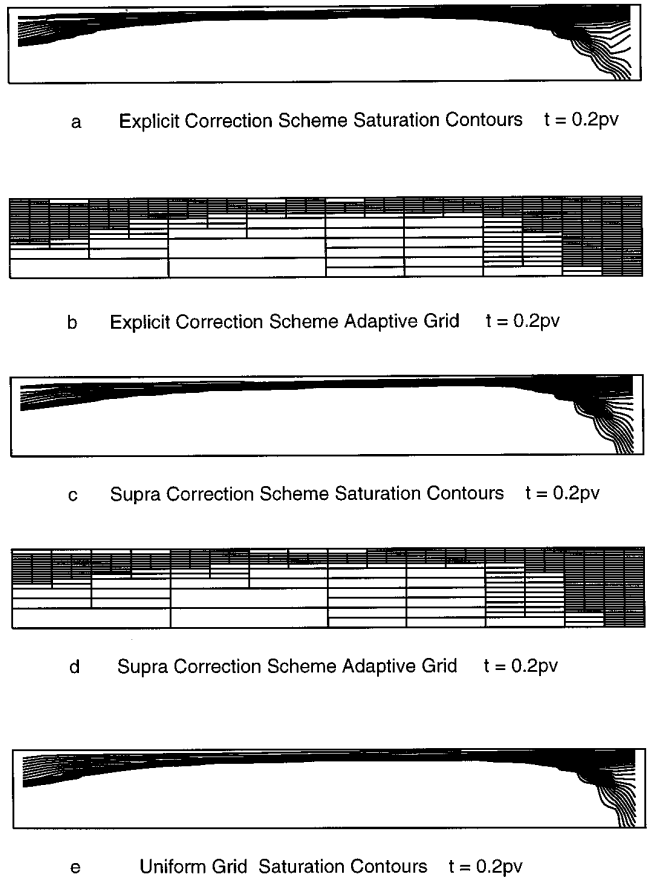

FIG. 16. Saturation field: Grid aspect ratio = 8; Isotropic permeability. Dynamically adaptive simulation. Corrected schemes vs Uniform grid.

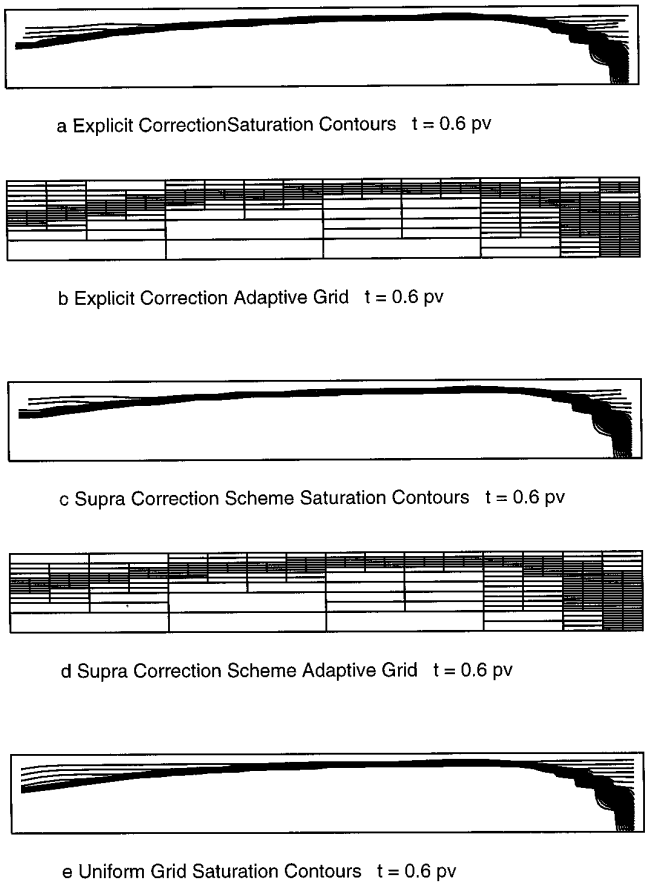

FIG. 17. Saturation field: Grid aspect ratio = 8; Isotropic permeability. Dynamically adaptive simulation. Corrected schemes vs Uniform grid.

anisotropic coefficients. Diagonal dominance is demonstrated for discrete locally isotropic spatially varying coefficients. Supra-convergence is demonstrated to $O(h)$ for an adaptive grid interface. The local fine cell interface velocity is formally $O(h)$ accurate. Support of the standard approximation is retained resulting in an easily implemented correction.

The new flux continuous correction is contrasted with a previously proposed correction, which requires increased support and is consequently complex to implement in a dynamic multilevel setting and has a nonsymmetric matrix. While both schemes remove the leading error the new scheme provides the most accurate results.

Computed convergence rates are presented for both of the corrected schemes and the uncorrected scheme. While the standard scheme exhibits convergence for problems where the error coefficient is minimized, the convergence rates deteriorate as the error coefficient increases. The new scheme exhibits the best convergence rates for all test cases in homogeneous and heterogeneous domains.

The contrast in results obtained by all schemes for fully dynamically adaptive simulations with transient flow are entirely consistent with the contrast in computed convergence rates. For problems with a minimum error coefficient the uncorrected standard scheme produces acceptable results; however, if the error coefficient is increased (for example, by choosing larger aspect ratios), the computed shock front is completely distorted by the grid-induced errors. The new adaptive scheme removes the errors and produces results which are comparable with equivalent uniformly fine grid simulations for all aspect ratio tests.

APPENDIX 1: DIAGONAL DOMINANCE (TEST FOR STANDARD CORRECTION)

The correction of Section 3 involves tangential interpolation of pressure to construct the appropriate normal flux. Away from the interface the standard scheme and properties prevail, thus only examination of the interface flux is required. The interpolated pressure is $(1 - \beta)p_a + \beta p_b$, where β is the interpolation coefficient and the corrected interface flux for cell a (Fig. 3 with c, d, b, replaced by a, b, c) is

$$w_{ab}(p_a - p_b) + w_{ac}((1 - \beta)p_a + \beta p_b - p_c),$$

where

$$w_{ab} = 2h_x k_{y_a} k_{y_b}/h_y(k_{y_a} + k_{y_b}),$$
$$w_{ac} = 2h_y k_{x_a} k_{x_c}/h_x(k_{x_a} + 2k_{x_c}).$$

Contributions to matrix coefficients of row a are

$$M_{aa} = w_{ab} + (1 - \beta)w_{ac}, \quad M_{ab} = \beta w_{ac} - w_{ab},$$
$$M_{ac} = -w_{ac}.$$

Diagonal dominance follows if

$$w_{ab} \geq \beta w_{ac}.$$

Linear interpolation equation (3.3) with $\beta = 1/4$, results in conditional diagonal dominance for spatially varying locally anisotropic or isotropic coefficients. However, for locally isotropic coefficients ($k_x = k_y$) use of Eq. (4.4) with $\beta = k_{x_b}/2(k_{x_a} + k_{x_b})$ results in

$$2(2 + k_{x_a}/k_{x_c}) \geq A_r^2,$$

demonstrating unconditional diagonal dominance for aspect ratios less than 2.

APPENDIX 2: SUPRA-CONVERGENCE

By transforming the new nonstandard interface operators acting on cell centered values into classical five point

operators acting on mean values supra-convergence at an adaptive grid interface is demonstrated with respect to mean values and then cell centered values.

For simplicity consider the new discretization of the pressure equation at a single interface and assume constant coefficients (although the analysis below will apply with sufficiently smooth variable coefficients). The discrete operator is obtained by applying the Gauss flux Theorem to Eq. (2.1) over each cell and introducing an appropriate approximation of the flux at each cell face. For an adaptive grid the new flux approximation of Eq. (5.3) is introduced at any adaptive interface. Referring to Fig. 5 with a and b replaced by fine grid indices (i, j), $(i, j-1)$, and c replaced by coarse grid indices $(I+1, J)$, respectively, the discrete operator for fine cell $(i, j-1)$ is

$$\begin{aligned} L_h p_h = \Bigg(& -\frac{2}{3}\frac{h_y}{h_x} k_x (p_{I+1,J} - (p_{ij} + p_{ij-1})/2) \\ & - k_y \frac{h_x}{h_y}(p_{i,j} - p_{ij-1}) \\ & + k_y \frac{h_x}{h_y}(p_{i,j-1} - p_{ij-2}) \\ & + k_x \frac{h_y}{h_x}(p_{i,j-1} - p_{i-1,j-1}) \Bigg) \Big/ h_x h_y = 0 \end{aligned} \tag{A.1a}$$

and for fine cell (i, j),

$$\begin{aligned} L_h p_h = \Bigg(& -\frac{2}{3}\frac{h_y}{h_x} k_x (p_{I+1,J} - (p_{ij} + p_{ij-1})/2) \\ & - k_y \frac{h_x}{h_y}(p_{i,j+1} - p_{ij}) + k_y \frac{h_x}{h_y}(p_{i,j} - p_{ij-1}) \\ & + k_x \frac{h_y}{h_x}(p_{i,j} - p_{i-1,j}) \Bigg) \Big/ h_x h_y = 0, \end{aligned} \tag{A.1b}$$

where (h_x, h_y) are the fine cell dimensions and (k_x, k_y) are the respective horizontal and vertical permeabilities. The discrete conservative operator L_h is related to the symmetric pressure matrix $\mathbf{M}$ by

$$\mathrm{diag}(A) L_h = \mathbf{M}, \tag{A.2}$$

where $\mathrm{diag}(A) = h_x h_y$ is the diagonal matrix of cell areas and L_h is symmetric in shape and nonsymmetric in coefficients for nonuniform grids. The first terms on the right-hand side of (A.1a) and (A.1b) are the same interface flux; the other terms are standard flux approximations.

The local fine grid interface velocities with respect to cells i,j and $i,j-1$ (denoted here by $v_{j\pm}$) at cell faces 1 and 2 are both approximated by the central interface velocity $v_{ij-1/2}$, so that, in addition to the central velocity error, a leading truncation error in velocity (denoted by $\tau^{\pm}_{\mathrm{vel}}$, where $\pm$ refers to the pair of fine interface cells) with respect to the fine cell faces is introduced. Performing a Taylor series expansion about the center of the interface and rearranging yields

$$\tau^{\pm}_{\mathrm{vel}} = v_{j\pm} - v_{ij-1/2} = \pm\frac{h_y}{2} v_y + \frac{h_y^2}{8} v_{yy} + O(h_y^3). \tag{A.3}$$

Since this velocity error is strictly local to the interface, then when calculating the truncation error $L_h P$ (where P is the exact solution), with respect to the fine cells i, j and i, $j-1$, a discrete difference in velocity normal to the interface creates an $O(1)$ truncation error. and thus the interface flux approximation contributes a leading truncation error of

$$\tau^{\pm}_h = \frac{\tau^{\pm}_{\mathrm{vel}}}{h_x} = \pm\frac{1}{2} A_r p_{xy} k_x + \frac{h}{8} A_r p_{xyy} k_x \tag{A.4}$$

to each of the fine cells. While the new flux approximation removes the $O(1/h)$ error convergence cannot be claimed according to (A.4) as $\tau^{\pm}_h$ is $O(1)$.

However, let us for the moment return to the interface velocity approximation Eq. (5.3). Working with the mean fine grid values and coarse grid values the discrete velocity can be written as

$$V_{ij-1/2} = -\frac{2}{3}\frac{h_y}{h_x} k_x (p_{I+1,J} - \overline{p}_{ij-1/2}), \tag{A.5}$$

where

$$\overline{p}_{ij-1/2} = (p_{i,j} + p_{i,j-1})/2.$$

With respect to the coarse grid cell $(I+1, J)$ the discrete scheme is

$$\begin{aligned} L_H p_H = \Bigg(& \frac{4}{3}\frac{h_y}{h_x} k_x (p_{I+1,J} - \overline{p}_{ij-1/2}) \\ & - k_y \frac{H_x}{H_y}(p_{I+1,J+1} - p_{I+1,J}) + k_y \frac{H_x}{H_y}(p_{I+1,J} - p_{I+1,J-1}) \\ & - k_x \frac{H_y}{H_x}(p_{I+2,J} - p_{I+1,J}) \Bigg) \Big/ H_x H_y = 0 \end{aligned}$$

which is a classical nonuniform grid five point approximation, where H refers to the coarse grid with cell dimensions (H_x, H_y). The error is second-order supra-convergent [20, 21] ($e_{I+1,J} = O(h^2)$); thus the velocity equation (A.5) is

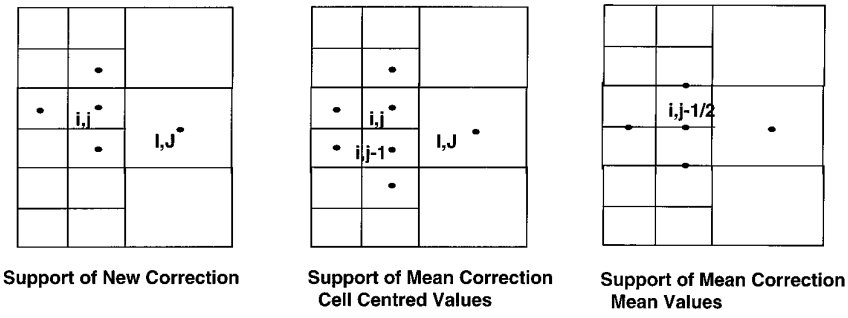

FIG. 18. Supra-convergence: Support of correction transformed to classical five point scheme interface $(i, j-1), (i, j)$.

second-order (super-convergent) at the midpoint between $(i, j-1/2)$ and (I, J).

This suggests examining the mean values of the solution on the fine grid. Refering to Fig. 18, a mean discrete operator (denoted here by μL_h) is obtained by adding the discrete equation (A.1a) for cell (i, j) to the adjacent discrete equation (A.1b) for cell $(i, j-1)$ at the interface to produce

$$\mu L_h p_h|_{ij-1/2} = \left(-\frac{2h_y}{3h_x} k_x (p_{I+1,J} - \overline{p}_{ij-1/2}) + k_x \frac{h_y}{h_x} (\overline{p}_{ij-1/2} - \overline{p}_{i-1j-1/2}) - k_y \frac{h_x}{h_y} (\overline{p}_{i,j+1/2} - 2\overline{p}_{ij-1/2} + \overline{p}_{i,j-3/2}) \right) \Big/ h_x h_y = 0, \tag{A.6}$$

where $\overline{p}_{ij\pm1/2}, \overline{p}_{ij+3/2}$ are mean values in the "y" direction of the finer grid defined by

$$\overline{p}_{ij+1/2} = (p_{i,j+1} + p_{i,j})/2 \tag{A.7}$$

The support of the mean discretisation with respect to the cell centered pressures is shown in Fig. 18. With respect to the mean values defined in (A.7) and the coarse grid values $p_{I+1,J}$, Eq. (A.6) is a classical five point approximation (with central node at $(i, j-1/2)$ (Fig. 18c) for the pressure equation on a nonuniform grid with mean error equation

$$\mu L_h \overline{e}_h|_{ij-1/2} = \tau_{nu}|_{ij-1/2},$$

where

$$\tau_{nu}|_{ij} = \frac{h_{x_{i+1,j}} - 2h_{x_{i,j}} + h_{x_{i-1,j}}}{4h_{x_{i,j}}} k_x p_{xx} + \frac{h_{y_{i,j+1}} - 2h_{y_{i,j}} + h_{y_{i,j-1}}}{4h_{y_{i,j}}} k_y p_{yy} \tag{A.8}$$

is the well-known error on a regular nonuniform grid [17] (here $h_{x_i} = h_{x_{i-1}} = h_x$, $h_{x_{i+1}} = 2h_x = H_x$, and $h_{y_{i,j+1}} - 2h_{y_i} + h_{y_{ij-1}} = 0$ as $h_{y_{i,j}}$ is constant in the y direction) and this scheme produces an $O(h^2)$ supra-convergent approximation [20, 21]. Hence,

$$\overline{e}_{ij-1/2} = O(h^2). \tag{A.9}$$

The definition of the discretisation with respect to the "mean" values is completed by defining an adjacent mean operator by addition of the discrete equations for cells (i, j) and $(i, j+1)$ to give

$$\mu L_h p_h|_{ij+1/2} = \left(-\frac{2h_y}{3h_x} k_x \frac{1}{2} (p_{I+1,J+1} - \overline{p}_{ij+3/2} + p_{I+1,J} - \overline{p}_{ij-1/2}) + k_x \frac{h_y}{h_x} (\overline{p}_{ij+1/2} - \overline{p}_{i-1j+1/2}) - k_y \frac{h_x}{h_y} (\overline{p}_{i,j+3/2} - 2\overline{p}_{ij+1/2} + \overline{p}_{i,j-1/2}) \right) \Big/ h_x h_y = 0. \tag{A.10}$$

The support of this discretisation with respect to cell centered pressures is shown in Fig. 19b. Since Eqs. (A.6) and (A.10) are obtained by row operations acting on the original discrete system they are equivalent to the original system and will produce identical results when solving for cell centered pressures. Equation (A.10) can also be written as a five point scheme in terms of mean values, together with a residual term. This can be seen by introducing the identities

$$\tfrac{1}{2}(p_{I+1,J+1} + p_{I+1,J}) = P_{I+1,J+1/2} + \tfrac{1}{2}\Delta_y^2 p_{I,J+1/2} \tag{A.11a}$$

on the coarse grid and

$$\tfrac{1}{2}(\overline{p}_{ij+3/2} + \overline{p}_{ij-1/2}) = \overline{p}_{ij+1/2} + \tfrac{1}{2}\Delta_y^2 \overline{p}_{ij+1/2} \tag{A.11b}$$

for mean fine grid values at stations which are aligned with the coarse grid, where Δ_y^2 is a (central) second difference

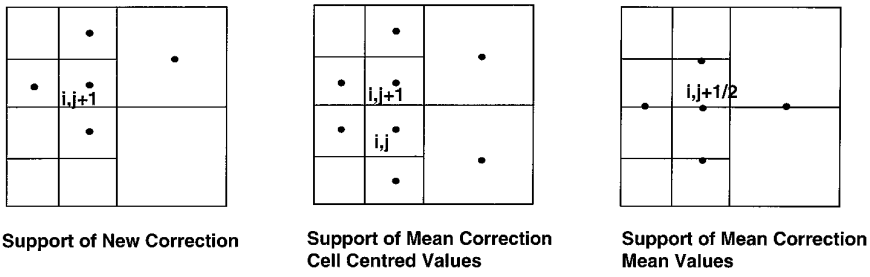

FIG. 19. Supra-convergence: Support of correction transformed to classical five point scheme interface (i, j), $(i, j + 1)$.

operator in y. Substituting (A.11) into (A.10) the discrete operator (A.10) can be rewritten as

$$\begin{aligned}\mu L_h\bar{p}|_{ij+1/2} = \Bigg(&-\frac{2h_y}{3h_x}k_x(p_{I+1,J+1/2} - \bar{p}_{ij+1/2}) \\ &+ k_x\frac{h_y}{h_x}(\bar{p}_{ij+1/2} - \bar{p}_{i-1j+1/2}) \\ &- k_y\frac{h_x}{h_y}(\bar{p}_{i,j+3/2} - 2\bar{p}_{ij+1/2} + \bar{p}_{i,j-1/2})\Bigg) \Big/ h_xh_y \\ &+ \frac{h_x}{6}k_xA_r^2\frac{\Delta_x}{h_x}\frac{\Delta_y^2}{h_y^2}p_{I+1/2,J+1/2} \\ = \hat{L}_h\bar{p}|_{ij+1/2} &+ h_x\frac{k_xA_r^2}{6}D^3_{yyx}\bar{p}|_{ij+1/2} = 0, \end{aligned} \tag{A.12}$$

where $\hat{L}_h$ is a classical nonuniform five point operator with respect to the mean fine grid values and mean coarse grid values with central node at $(i, j + 1/2)$ (Fig. 19c), Δ_x is a central difference operator in x and D^3_{yyx} is a third-order divided difference operator. Substitution of the exact solution into (A.12) reveals a truncation error,

$$\begin{aligned}\mu L_hP|_{ij+1/2} &= \hat{L}_hP|_{ij+1/2} + h_x\frac{k_xA_r^2}{6}D^3_{yyx}P|_{ij+1/2} \\ &= \tau_{nu}|_{ij+1/2} + h_x\frac{k_xA_r^2}{6}P_{yyx}.\end{aligned} \tag{A.13}$$

Subtracting (A.12) from (A.13) and, rearranging, the error equation corresponding to Eq. (A.10) can be written as

$$\hat{L}_h\bar{e}_h|_{ij+1/2} = \tau_{nu}|_{ij+1/2} + h_x\frac{k_xA_r^2}{6}D^3_{yyx}p|_{ij+1/2}, \tag{A.14}$$

where the residual translates into an additional term of $O(h)$ on the right-hand side, together with the usual nonuniform grid error (cf. (A.8)). Supra-convergence arguments [20, 21] can be used to show that the mean error is now $O(h)$; thus,

$$\bar{e}_{ij+1/2} = O(h). \tag{A.15}$$

By Eq. (A.7) in the field the mean errors are related to the cell centered errors through

$$\bar{e}_{ij-1/2} = \frac{e_{ij} + e_{ij-1}}{2} + \frac{h^2}{8}P_{yy}. \tag{A.16}$$

At the boundary the mean error and cell centered discretization error are identical by reflection conditions; thus the cell centered errors are obtained from (A.16) by backward substitution and they are at most $O(h)$. From Eqs. (A.9) and (A.15) it follows that the mean errors are supra-convergent in an oscillatory fashion such that $O(h^2) \le \bar{e}_{ij} \le O(h)$ and by (A.16) the cell centered leading errors are $\pm O(h)$ with a mean value cancellation to $O(h^2)$ at each local interface, e.g., at $ij - 1/2$ (Fig. 18a). In addition, the actual interface velocity used in the discretization is defined by the difference of $O(h^2)$ mean values (corresponding to (A.5)) which suggests that, while the formal pointwise error in velocity at the fine grid interfaces can only be $O(h)$ upon integration, the velocity error norm satisfies $O(h^2) \le \|V - V_h\| \le O(h)$.

APPENDIX 3: FLUX CONTINUITY FOR ARBITRARY REFINEMENT RATIO

Construction of a flux continuous scheme which maintains the standard scheme support and matrix structure is illustrated below for $G_r = 4$. Referring to Fig. 6 the equations which define the interface pressures $p1$, $p2$ are obtained by imposing flux continuity, using the piecewise constant pressure gradient of triangle 1.2.r to define the right-hand side flux at positions 1 and 2,

$$\begin{aligned}k_a(p_1 - p_a)/h_x &= k_r(Ap_r + Bp_1 + Cp_2) \\ k_b(p_2 - p_b)/h_x &= k_r(Ap_r + Bp_1 + Cp_2),\end{aligned}$$

where A, B, and C are standard geometric factors [25]. This procedure is generalised for an arbitrary interface

by using disjoint triangles (sharing common vertex r) to construct the flux which ensures that scheme support does not extend beyond nearest neighbours. Other ways of constructing flux continuous schemes are possible; however, scheme support is increased.

ACKNOWLEDGMENTS

I thank Mike Christie for his support of this project. I am grateful for the referees, constructive comments, and review of this paper.

REFERENCES

1. P. Quandalle and P. Besset, ''Reduction of Grid Effects Due to Local SubGridding in Simulations Using a Composite Grid,'' SPE 13527, 1985, in *Reservoir Simulation Symposium, Dallas, TX, February* 10–13, p. 295.
2. M. G. Edwards, ''A Dynamically Adaptive Godunov Scheme for Reservoir Simulation on Large Aspect Ratio Grids,'' in *Proceedings, Conference on Numerical Methods for Fluid Dynamics, Reading Univ., UK, April 7–10,* edited by K. W. Morton and M. J. Baines.
3. P. A. Forsyth and P. H. Sammon, ''Local Mesh Refinement and Modelling of Faults and Pinchouts,'' SPE 13534, in *Reservoir Simulation Symposium, Dallas, TX, February* 10–13, 1985, p. 267.
4. D. U. von Rosenberg, ''Local Mesh Refinement for Finite Difference Methods,'' SPE 10974, 1982 (unpublished).
5. Z. E. Heinemann, ''Using Local Grid Refinement in a Multiple-Application Reservoir Simulator,'' SPE 12255, 1983 (unpublished).
6. D. K. Han, D. L. Han, C. Z. Yan, and L. T. Peng, ''A More Flexible Approach of Dynamic Local Grid Refinement for Reservoir Modeling,'' SPE 16014, 1987 (unpublished).
7. M. L. Wasserman ''Local Grid Refinement for Three Dimensional Simulators,'' SPE 16013, 1987 (unpublished).
8. G. H. Schmidt and F. J. Jacobs, *J. Comput. Phys.* **77,** 140 (1988).
9. E. C. Nacul and K. Aziz, ''Efficient Use of Domain Decomposition and Local Grid Refinement in Reservoir Simulation,'' SPE 20740, 1990 (1990).
10. W. A. Mulder and R. H. J. GmeligMeyling, ''Numerical Simulation of Two-Phase Flow Using Locally Refined Grids in Three-Space Dimensions,'' SPE 21230, 1991 (unpublished).
11. F. X. Deimbacher and Z. E. Heinemann, ''Time Dependent Incorporation of Locally Irregular Grids in Large Reservoir Simulation Models,'' SPE 25260, in *Twelfth SPE Reservoir Simulation Symposium, New Orleans, LA, Feb 28–March 3, 1993.*
12. M. G. Edwards, ''A Dynamically Adaptive Higher Order Godunov Scheme For Reservoir Simulation In Two Dimensions,'' in *3rd European Conference on the Mathematics of Oil Recovery, Delft University 17–19 June 1992,* edited by M. A. Christie, F. V. Da Silva, C. L. Farmer, O. Guillon, Z. E. Heinmann, P. Lemonnier, J. M. M. Regtien, and E. van Spronson, p. 239.
13. M. G. Edwards and M. A. Christie, ''Dynamically Adaptive Godunov Schemes With Renormalization for Reservoir Simulation,'' SPE 25268, in *Twelfth SPE Reservoir Simulation Symposium, New Orleans, LA, Feb.* 28–*Mar.* 3, 1993, p. 413.
14. M. G. Edwards, to appear.
15. M. G. Edwards, ''A Flux Continuous Approximation of the Pressure Equation for *h*-Adaptive Grids,'' in *MAFELAP, The Mathematics of Finite Elements and Applications. Brunel, April 93,* edited by J. R. Whiteman (Wiley, New York, 1993).
16. L. Demkowicz and J. T. Oden, TICOM Report 88-02, Univ. of Texas, Austin, TX, 1988 (unpublished).
17. K. Aziz and A. Settari, ''Petroleum Reservoir Simulation,'' Elsevier Applied Science, New York.
18. P. Wesseling, ''Linear Multigrid Methods'' in *Multigrid Methods,* Frontiers in Applied Mathematics, edited by S. F. McCormick (SIAM, Philadelphia, 1987).
19. H. O. Kreiss, T. A. Manteuffel, B. Swartz, B. Wendroff, and A. B. White, *Math. Comput.* **47,** 537 (1986).
20. A. Weiser and M. F. Wheeler *SIAM J. Numer. Anal.* **25,** 351 (1988).
21. P. A. Forsyth and P. H. Sammon, *Appl. Numer. Math.* **4,** 377 (1988).
22. I. Yotov, M. F. Wheeler, and T. Arbogast, private communication.
23. M. G. Edwards, in preparation.
24. J. B. Bell, P. Colella, and J. A. Trangenstein, *J. Comput. Phys.* **82,** 362 (1989).
25. E. B. Becker, G. F. Carey, and J. T. Oden, *Finite Elements an Introduction,* Vol. 1 (Prentice–Hall, Englewood Cliffs, NJ, 1981).